DOI: 10.1021/cg100200b

CRYSTAL GROWTH & DESIGN Article

2010, Vol. 10
5034–5042

Metal-Involved Solvothermal Interconversions of Pyrazinyl Substituted Azole Derivatives: Controllability and Mechanism

Cheng-Peng Li, Xiao-Hu Zhao, Xu-Dong Chen, Qian Yu, and Miao Du*

College of Chemistry and Life Science, Tianjin Key Laboratory of Structure and Performance for Functional Molecule, Tianjin Normal University, Tianjin 300387, P. R. China

Received February 8, 2010; Revised Manuscript Received September 8, 2010

ABSTRACT: Under different solvothermal reaction conditions **I** (60 °C for 48 h) and **II** (140 °C for 72 h), the dipyrazinyl compounds bearing oxadiazole and triazole spacers, that is, 2,5-bis(2-pyrazinyl)-1,3,4-oxadiazole ($\mathbf{L^1}$) and 4-amino-3,5-bis-(2-pyrazinyl)-1,2,4-triazole ($\mathbf{L^2}$), may suffer reversible conversions in the presence of certain metal salts. Other related derivatives such as 3,5-bis(2-pyrazinyl)-1,2,4-triazole-4-yl-*N*-pyrazinamide ($\mathbf{HL^4}$) and pyrazine-2-carboxylic acid ($\mathbf{HL^0}$) can also be (in situ) obtained from $\mathbf{L^1}$ and $\mathbf{L^2}$, respectively, under conditions **I** and **II**. Beyond this, *N*,*N*′-bis(2-pyrazineamide) ($\mathbf{H_2L^3}$) can be in situ afforded from both precursors $\mathbf{L^1}$ and $\mathbf{L^2}$, and thus, may be considered as the potential intermediate during the interconversions. The possible mechanisms and influence factors of these reactions have also been established based on the experimental results. As a result, a variety of crystalline materials (co-crystals and coordination complexes) with attractive supramolecular architectures have been isolated by regulating the reaction conditions well (reaction temperature, metal ion, and even inorganic counteranion).

Introduction

The solvothermal synthesis method has been widely used as a promising technique for preparing multifarious inorganic−organic hybrid solids,[1,2] such as metal−organic frameworks,[3] superionic conductors and complex fluorides,[4] magnetic materials,[5] as well as luminescence phosphors,[6] and so on. Recently, this strategy has also been applied to facilitate the production of new coordination crystalline materials via in situ solvothermal metal/ligand reactions, which are usually unreachable by the conventional synthetic routes.[1a,7] However, in this context, the reaction mechanism under such complicated synthetic conditions is still a scientific problem to be solved urgently. Of further importance, the related results may be helpful for the rational preparation of new materials by effectively controlling the reaction conditions.

Derivatives of azole systems have been of growing research interest, which can serve as precursors for a number of *N*-heterocycles,[8] as well as be used in pharmaceuticals as metabolically stable surrogates of carboxylic acids and lipophilic spacers, and in photography and information recording systems.[9] Among them, compounds with oxadiazole and triazole groups that may have different dispositions of the heteroatoms on the 5-membered rings also show interesting coordination behaviors.[10,11]

In this regard, we have systematically investigated the coordination chemistry of a series of dipyridyl derivatives with oxadiazole or triazole spacers.[10a,12] Also, the related dipyrazinyl ligands may be of further interest due to the changeful binding fashion of pyrazinyl in comparison with that of pyridyl. From the viewpoint of organic synthesis, the dipyrazinyl compounds 2,5-bis(2-pyrazinyl)-1,3,4-oxadiazole ($\mathbf{L^1}$) and 4-amino-3,5-bis(2-pyrazinyl)-1,2,4-triazole ($\mathbf{L^2}$) can be prepared by using multistep procedures, which usually involve hydrazine derivatives as the starting reagents.[13] In fact, the reaction pathways for synthesizing $\mathbf{L^1}$ and $\mathbf{L^2}$ are similar except the slightly changed reaction conditions such as temperature (140 °C for $\mathbf{L^1}$ and 130 °C for $\mathbf{L^2}$) and atmosphere (air for $\mathbf{L^1}$ and inert gas for $\mathbf{L^2}$). It seems that there are some potential connections between such two compounds, and the possible intermediates during the formation of $\mathbf{L^1}$ and $\mathbf{L^2}$ are suggested to be *N*,*N*′-bis(2-pyrazineamide) ($\mathbf{H_2L^3}$) and 3,6-bis(2-pyrazinyl)-1,2-dihydro-1,2,4,5-tetrazine, respectively.[13b]

Recently, Chen et al. have established a reliable synthetic method for diverse coordination complexes with 1,2,4-triazole and its derivatives, by using in situ solvothermal metal/ligand reactions from organonitriles.[11a,14] However, at this stage, a clear understanding of the "bridge" between 1,3,4-oxadiazole and 1,2,4-triazole compounds remains unexplored. It is significant to demonstrate their possible interconvertibility under certain conditions and the exact information for the intermediate products, which will provide new insights into not only the mechanisms of such organic reactions but also preparing novel coordination complexes. In this work, by accurately controlling the reaction conditions, we have successfully (in situ) isolated a series of related dipyrazinyl-based systems by using the solvothermal synthetic method. These trials illuminate the interconvertible paths between such organic azole compounds with the assistance of certain metal ions. The possible reaction mechanism and intermediate as well as the supramolecular structures of the crystalline products will also be presented.

Experimental Section

Materials and Physical Measurements. With the exception of 2,5-bis(2-pyrazinyl)-1,3,4-oxadiazole ($\mathbf{L^1}$) and 4-amino-3,5-bis(2-pyrazinyl)-1,2,4-triazole ($\mathbf{L^2}$), which were synthesized according to the reported procedures,[13] all reagents were obtained commercially and used as received. Distilled water was used throughout. Elemental analyses of C, H, and N were taken on a CE-440 (Leemanlabs) analyzer. Fourier transform (FT) IR spectra (KBr pellets) were taken on an AVATAR-370 (Nicolet) spectrometer. ^{1}H NMR spectra were performed on a Bruker AV 300 spectrometer,

*To whom correspondence should be addressed. E-mail: dumiao@public.tpt.tj.cn.

Published on Web 10/28/2010

and the chemical shifts were reported in ppm with respect to the reference standards. High resolution mass spectra were measured on a Finnigan GC-MS-4021 spectrometer. X-ray photoelectron spectroscopy (XPS) analysis was performed on a Kratos Axis Ultra DLD multi-technique spectrometer with a monochromated Al-Ka X-ray source. Variable-temperature magnetic susceptibilities were measured by using a MPMS-7 SQUID magnetometer. Diamagnetic corrections were made with Pascal's constants for all constituent atoms. Abbreviations: DMF = *N*,*N*-dimethylformamide, DMSO = dimethyl sulfoxide, $\mathbf{HL^4}$ = 3,5-bis(2-pyrazinyl)-1,2,4-triazole-4-yl-*N*-pyrazinamide, H_3TMA = trimesic acid.

General Synthetic Procedure for Condition I. A mixture of the starting reagents in H_2O-DMF (v/v = 1:1, 10 mL) was placed into a Parr Teflon-lined stainless steel vessel (20 mL) under autogenous pressure, which was heated at 60 °C for 48 h and then cooled to room temperature at a rate of 5 °C/h. The resulting crystalline products were isolated by filtration, washed with a small amount of water, and dried in air.

$\mathbf{L^2}$. Starting reagents: $\mathbf{L^1}$ (23 mg, 0.1 mmol) and $Zn(NO_3)_2\cdot 6H_2O$ (30 mg, 0.1 mmol). Dark-brown lamellar crystals were collected in 42% yield (5 mg, based on $\mathbf{L^1}$). Anal. Calcd for $C_{10}H_8N_8$: C, 50.00; H, 3.36; N, 46.64%. Found: C, 49.86; H, 3.30; N, 46.43%. IR (cm^{-1}): 3319m, 3232m, 1573s, 1543m, 1464w, 1407s, 1386s, 1316w, 1291w, 1145s, 1087s, 1018vs, 971s, 863s, 754m, 702w, 583w, 489w. ^1H NMR (DMSO, ppm): δ = 7.03 (s, 2H), 8.84 (s, 4H), 9.39 (s, 2H). EI-MS: m/z 240 $[M]^+$.

$\mathbf{HL^4\cdot H_2O}$. Starting reagents: $\mathbf{L^1}$ (23 mg, 0.1 mmol) and $ZnSO_4\cdot 7H_2O$ (29 mg, 0.1 mmol). Colorless block crystals were collected in 38% yield (7 mg, based on $\mathbf{L^1}$). Anal. Calcd for $C_{15}H_{12}N_{10}O_2$: C, 49.45; H, 3.32; N, 38.45%. Found: C, 49.76; H, 3.43; N, 38.25%. IR (cm^{-1}): 3509s, 3323m, 3237m, 1701vs, 1652w, 1581w, 1510s, 1462m, 1405s, 1320w, 1297w, 1163s, 1126m, 1079w, 1049w, 1017s, 975w, 921w, 858w, 815w, 751w, 699m, 637w, 570w, 488w. ^1H NMR (DMSO, ppm): δ = 4.59 (s, 2H), 8.65 (s, 4H), 8.77 (s, 2H), 9.21 (s, 1H), 9.38 (s, 2H), 13.53 (s, 1H). EI-MS: m/z 346 $[M]^+$ ($\mathbf{HL^4}$).

$[(\mathbf{H_3TMA})\cdot(\mathbf{L^2})]$ (1). Starting reagents: H_3TMA (21 mg, 0.1 mmol), $\mathbf{L^1}$ (23 mg, 0.1 mmol), and $Zn(NO_3)_2\cdot 6H_2O$ (30 mg, 0.1 mmol). Colorless block crystals were obtained in 27% yield (6 mg, based on $\mathbf{L^1}$). Anal. Calcd for $C_{19}H_{14}N_8O_6$: C, 50.67; H, 3.13; N, 24.88%. Found: C, 50.82; H, 3.34; N, 24.65%. IR (cm^{-1}): 3332m, 3240w, 2801s, 2526s, 1872w, 1701vs, 1592w, 1554m, 1450m, 1412m, 1388m, 1320w, 1238vs, 1179s, 1143vs, 1095m, 1045m, 1020s, 982s, 928m, 860m, 743s, 676s, 653m, 586w, 503w. ^1H NMR (DMSO, ppm): δ = 7.56 (s, 2H), 8.65 (s, 3H), 8.87 (s, 4H), 9.34 (s, 2H), 12.77 (s, 3H).

$[(\mathbf{H_3TMA})\cdot(\mathbf{HL^4})]\cdot\mathbf{H_2O}$ (2). Starting reagents: H_3TMA (21 mg, 0.1 mmol), $\mathbf{L^1}$ (23 mg, 0.1 mmol), and $ZnSO_4\cdot 7H_2O$ (29 mg, 0.1 mmol). Pale-red lamellar single crystals were obtained in 38% yield (11 mg, based on $\mathbf{L^1}$). Anal. Calcd for $C_{24}H_{18}N_{10}O_8$: C, 50.18; H, 3.16; N, 24.38%. Found: C, 50.36; H, 3.35; N, 24.57%. IR (cm^{-1}): 3257s, 3078m, 2892s, 2524m, 1710vs, 1489m, 1406s, 1258s, 1235s, 1163s, 1101s, 1051m, 1018s, 981w, 927w, 861w, 740w, 699w, 672m, 584w, 522w, 479w. ^1H NMR (DMSO, ppm): δ = 4.68 (s, 2H), 8.62 (s, 3H), 8.73 (s, 4H), 8.82 (s, 2H), 9.25 (s, 1H), 9.35 (s, 2H), 12.82 (s, 3H), 13.57 (s, 1H).

$\{[\mathbf{Cu_3(L^4)_2(SO_4)_2(H_2O)_3}](\mathbf{H_2O})_9\}_n$ (3). Starting reagents: $\mathbf{L^1}$ (23 mg, 0.1 mmol) and $CuSO_4\cdot 5H_2O$ (25 mg, 0.1 mmol). Green block crystals were obtained in 25% yield (8 mg, based on $\mathbf{L^1}$). Anal. Calcd for $C_{30}H_{42}Cu_3N_{20}O_{22}S_2$: C, 27.94; H, 3.28; N, 21.72%. Found: C, 28.13; H, 3.15; N, 21.91%. IR (cm^{-1}): 3435bs, 3081w, 1672s, 1624vs, 1483w, 1449w, 1418w, 1386w, 1314m, 1153m, 1044m, 992w, 858w, 756w, 717w, 619w, 512w, 464w.

$[\mathbf{Co^{III}_2(L^3)_3}](\mathbf{H_2O})_{7.5}$ (4). Starting reagents: $\mathbf{L^1}$ (23 mg, 0.1 mmol) and $Co(NO_3)_2\cdot 6H_2O$ (29 mg, 0.1 mmol). Dark-red lamellar crystals were obtained in 28% yield (9 mg, based on $\mathbf{L^1}$). Anal. Calcd for $C_{30}H_{33}Co_2N_{18}O_{13.5}$: C, 36.78; H, 3.40; N, 25.74%. Found: C, 36.69; H, 3.55; N, 25.89%. IR (cm^{-1}): 3431bs, 3067m, 1638vs, 1587s, 1472w, 1426w, 1352s, 1286m, 1168s, 1055m, 952w, 862w, 777w, 594w, 504w.

General Synthetic Procedure for Condition II. A mixture of the starting reagents in H_2O-DMF (v/v = 1:1, 10 mL) was placed into a Parr Teflon-lined stainless steel vessel (20 mL) under autogenous pressure, which was heated at 140 °C at 72 h and then cooled to room temperature at a rate of 5 °C/h. The resulting crystalline products were isolated by filtration, washed with a small amount of water, and dried in air.

$[\mathbf{Co^{III}_2(L^3)_3}](\mathbf{H_2O})_{7.5}$ (4). Starting reagents: $\mathbf{L^2}$ (24 mg, 0.1 mmol) and $Co(NO_3)_2\cdot 6H_2O$ (29 mg, 0.1 mmol). Dark-red lamellar crystals were obtained in 21% yield (7 mg, based on $\mathbf{L^2}$). Anal. Calcd for $C_{30}H_{33}Co_2N_{18}O_{13.5}$: C, 36.78; H, 3.40; N, 25.74%. Found: C, 36.56; H, 3.72; N, 25.87%. IR (cm^{-1}): 3425bs, 3063s, 1638vs, 1586s, 1470w, 1426m, 1353s, 1285m, 1169m, 1055m, 949w, 864m, 777w, 595w, 502w.

$[\mathbf{Co(L^1)_2(SCN)_2(H_2O)_2}](\mathbf{L^1})_2(\mathbf{H_2O})_6$ (5). Starting reagents: $\mathbf{L^2}$ (24 mg, 0.1 mmol), NH_4SCN (8 mg, 0.1 mmol), and $Co(NO_3)_2\cdot 6H_2O$ (29 mg, 0.1 mmol). Red block crystals were obtained in 39% yield (12 mg, based on $\mathbf{L^2}$). Anal. Calcd for $C_{42}H_{40}CoN_{26}O_{12}S_2$: C, 41.21; H, 3.29; N, 29.75%. Found: C, 41.03; H, 3.19; N, 29.92%. IR (cm^{-1}): 3431m, 2083m, 2050vs, 1669vs, 1569m, 1503w, 1473w, 1417m, 1384m, 1311s, 1277s, 1188m, 1142vs, 1094m, 1059s, 933m, 855m, 775w, 754w, 727w, 702w, 655w, 500m, 458w.

$[\mathbf{Cu^ICu^{II}(L^1)(L^3)(SCN)}]_2(\mathbf{DMF})_2$ (6a). Starting reagents: $\mathbf{L^2}$ (24 mg, 0.1 mmol), NH_4SCN (8 mg, 0.1 mmol), and $Cu(NO_3)_2\cdot 3H_2O$ (24 mg, 0.1 mmol). Red block crystals were obtained in 17% yield (12 mg, based on $\mathbf{L^2}$). Anal. Calcd for $C_{48}H_{38}Cu_4N_{28}O_8S_2$: C, 39.67; H, 2.64; N, 26.99%. Found: C, 39.82; H, 2.46; N, 27.09%. IR (cm^{-1}): 3059w, 2924m, 2067s, 1657vs, 1536s, 1426w, 1427w, 1383s, 1285w, 1239w, 1157m, 1037m, 856w, 767w, 578w, 497w, 460w.

$[\mathbf{Cu^ICu^{II}(L^1)(L^3)(SCN)}]_2(\mathbf{DMF})_2(\mathbf{H_2O})_2$ (6b). Starting reagents: $\mathbf{L^2}$ (24 mg, 0.1 mmol), NH_4SCN (8 mg, 0.1 mmol), and $CuCl_2\cdot 2H_2O$ (17 mg, 0.1 mmol). Red block crystals were obtained in 19% yield (14 mg, based on $\mathbf{L^2}$). Anal. Calcd for $C_{48}H_{42}Cu_4N_{28}O_{10}S_2$: C, 38.71; H, 2.84; N, 26.33%. Found: C, 38.51; H, 2.71; N, 26.49%. IR (cm^{-1}): 3439s, 2921m, 2067s, 1657vs, 1538s, 1465w, 1385s, 1278w, 1193m, 1154s, 1041m, 759w, 617w, 556w, 516w, 464w.

General Synthetic Procedure for Condition III. A mixture of the starting reagents in H_2O-DMF (v/v = 1:1, 10 mL) was stirred and heated at 60 °C for 30 min. The resulting solution was cooled to room temperature and filtered. The filtrate was allowed to stand at room temperature, affording well-shaped single crystals suitable for X-ray diffraction analysis upon slow solvent evaporation. The products were isolated by filtration, washed with a small amount of water, and dried in air.

$[\mathbf{Co(L^2)_2(SCN)_2}]$ (7). Starting reagents: $\mathbf{L^2}$ (24 mg, 0.1 mmol), NH_4SCN (8 mg, 0.1 mmol), and $CoCl_2\cdot 6H_2O$ (24 mg, 0.1 mmol). Red block single crystals were collected in 43% yield (14 mg, based on L^2). Anal. Calcd for $C_{22}H_{16}CoN_{18}S_2$: C, 40.31; H, 2.46; N, 38.46%. Found: C, 40.11; H, 2.59; N, 38.56%. IR (cm^{-1}): 3273m, 3197m, 3056w, 2084vs, 1683w, 1590w, 1481w, 1442m, 1400m, 1378m, 1292w, 1183m, 1140w, 1027s, 859w, 774w, 703w, 668w, 489w.

$[\mathbf{Mn(L^2)(SCN)_2(H_2O)}]_2(\mathbf{H_2O})_2$ (8). Starting reagents: $\mathbf{L^2}$ (24 mg, 0.1 mmol), NH_4SCN (8 mg, 0.1 mmol), and $MnCl_2\cdot 4H_2O$ (20 mg, 0.1 mmol). Yellow block crystals were collected in 49% yield (11 mg, based on $\mathbf{L^2}$). Anal. Calcd for $C_{24}H_{24}Mn_2N_{20}O_4S_4$: C, 32.22; H, 2.70; N, 31.31%. Found: C, 32.31; H, 2.55; N, 31.45%. IR (cm^{-1}): 3456b, 3215m, 3153m, 2066vs, 1607w, 1548w, 1500m, 1478m, 1408m, 1276m, 1198m, 1133w, 1029s, 808w, 769w, 699w, 656w.

X-ray Crystallography. Single-crystal X-ray diffraction data for all compounds were collected on a Bruker Apex II CCD diffractometer at room temperature with Mo Kα radiation (λ = 0.71073 Å). In each case, there was no evidence of crystal decay during data collection. A semiempirical absorption correction was applied (SADABS), and the program SAINT was used for integration of the diffraction profiles.[15] All structures were solved by direct methods using the SHELXS program of the SHELXTL package and refined with SHELXL.[16] The non-H atoms were modeled with anisotropic thermal parameters and refined by full-matrix least-squares methods on F^2. In general, C-bound H atoms were placed geometrically and refined as riding, whereas O- and N-bound H atoms were first located in difference Fourier maps, and then fixed at the calculated sites. For **3**, the hydrogen atoms for all water molecules were not located (O22 was refined isotropically). For **4**, all lattice water moieties are located at the special positions and disordered over two sites (see CIF for details) with pseudoisotropic restraint (ISOR) used in the refinement. Thus, the affiliated H atoms were not determined. For **6b**, both pseudoisotropic and standard geometry constraints were used for the lattice DMF. In addition, the lattice

Table 1. Crystallographic Data and Structural Refinement Summary for L^2, $HL^4 \cdot H_2O$, and 1−8

	L^2	$HL^4 \cdot H_2O$	1	2	3	4
empirical formula	$C_{10}H_8N_8$	$C_{15}H_{12}N_{10}O_2$	$C_{19}H_{14}N_8O_6$	$C_{24}H_{18}N_{10}O_8$	$C_{30}H_{42}Cu_3N_{20}O_{22}S_2$	$C_{30}H_{33}Co_2N_{18}O_{13.5}$
M_r	240.24	364.35	450.38	574.48	1289.58	979.60
crystal system	triclinic	triclinic	monoclinic	triclinic	monoclinic	trigonal
space group	$P\bar{1}$	$P\bar{1}$	$P2_1/c$	$P\bar{1}$	$P2_1$	$R3\bar{c}$
a/Å	6.251(2)	7.152(1)	18.39(1)	8.361(7)	7.529(2)	12.7276(9)
b/Å	6.790(2)	11.476(2)	7.152(5)	11.40(1)	21.071(3)	12.7276(9)
c/Å	12.781(4)	11.863(2)	14.98(1)	13.72(1)	14.626(2)	43.053(6)
α/°	85.939(4)	118.206(2)		75.02(1)		
β/°	80.652(4)	91.590(2)	96.92(1)	85.49(1)	94.40(2)	
γ/°	72.413(3)	103.497(2)		88.14(1)		
V/Å^3	510.1(3)	823.4(2)	1955(3)	1259(2)	2313.5(8)	6040(1)
Z	2	2	4	2	2	6
ρ_{calcd}/g cm^{-3}	1.564	1.469	1.530	1.515	1.851	1.616
$F(000)$	248	376	928	592	1314	3006
μ/mm^{-1}	0.109	0.107	0.118	0.118	1.563	0.912
total/independent reflns	2784/1783	4492/2883	10087/3455	6801/4366	9270/5101	9841/1191
R_{int}	0.0149	0.0144	0.0473	0.0283	0.0644	0.0651
R^a, wR^b	0.0337, 0.0895	0.0346, 0.0969	0.0491, 0.1014	0.0444, 0.1057	0.0501, 0.1240	0.0442, 0.1315
GOF	1.039	1.067	1.005	1.084	1.101	1.024
residuals/e Å^{-3}	0.136, −0.153	0.235, −0.218	0.279, −0.268	0.278, −0.222	1.279, −0.908	0.715, −0.293

	5	6a	6b	7	8
empirical formula	$C_{42}H_{40}CoN_{26}O_{12}S_2$	$C_{48}H_{38}Cu_4N_{28}O_8S_2$	$C_{48}H_{42}Cu_4N_{28}O_{10}S_2$	$C_{22}H_{16}CoN_{18}S_2$	$C_{24}H_{24}Mn_2N_{20}O_4S_4$
M_r	1224.07	1453.31	1489.38	655.58	894.75
crystal system	triclinic	triclinic	monoclinic	monoclinic	triclinic
space group	$P\bar{1}$	$P\bar{1}$	$C2/c$	$P2_1/c$	$P\bar{1}$
a/Å	7.4346(9)	10.914(2)	22.843(4)	9.146(2)	8.283(1)
b/Å	12.850(2)	11.727(2)	14.947(3)	9.251(2)	9.545(1)
c/Å	14.618(2)	12.808(2)	19.278(4)	15.856(4)	11.779(2)
α/°	72.193(2)	80.213(2)			89.581(2)
β/°	79.256(2)	66.379(2)	97.710(3)	98.041(3)	76.333(2)
γ/°	88.374(2)	72.096(2)			84.805(2)
V/Å^3	1305.7(3)	1427.2(3)	6523(2)	1328.5(5)	901.0(2)
Z	1	1	4	2	1
ρ_{calcd}/g cm^{-3}	1.557	1.691	1.517	1.639	1.649
$F(000)$	629	734	3016	666	454
μ/mm^{-1}	0.496	1.623	1.425	0.857	0.997
total/independent reflns	7120/4526	7803/5020	17538/5756	5646/2341	4950/3139
R_{int}	0.0197	0.0246	0.0639	0.0203	0.0156
R^a, wR^b	0.0449, 0.1198	0.0423, 0.0997	0.0636, 0.1727	0.0289, 0.0699	0.0287, 0.0756
GOF	1.065	1.025	1.007	1.060	1.066
residuals/e Å^{-3}	0.452, −0.399	0.618, −0.416	0.860, −0.476	0.264, −0.188	0.263, −0.244

$^a R = \Sigma||F_o| - |F_c||/\Sigma|F_o|$. $^b wR = [\Sigma[w(F_o^2 - F_c^2)^2]/\Sigma w(F_o^2)^2]^{1/2}$.

water is disordered over two positions (see CIF in Supporting Information for details) and the affiliated H atoms were not determined. Further details for crystallographic data and refinement conditions are listed in Table 1. Selected bond parameters and H-bonding geometries are shown in Tables S1 and S2, respectively.

Results and Discussion

Transformation from the Oxadiazole Derivative (L^1). All reactions were performed under condition **I** (solvothermal, 60 °C for 48 h, see Scheme 1). When $Zn(NO_3)_2$ is used to react with L^1, the crystalline product is confirmed to be L^2. In fact, the single crystals of L^2 are difficult to obtain by a direct recrystallization of L^2, although a large number of experiments have been attempted using different solvents. However, notably, recrystallization of L^2 in the presence of $Zn(OAc)_2$ readily affords the single crystals of L^2.[17] Our further results show that the similar transition from L^1 to L^2 can also be realized by using $Zn(OAc)_2$ or $ZnCl_2$ as the starting reagent, instead of $Zn(NO_3)_2$. Remarkably, when $ZnSO_4$ is used in such a course, a more complicated compound $HL^4 \cdot H_2O$ (HL^4 = 2,5-bis(2-pyrazin-yl)-1,2,4-triazole-4-yl-*N*-pyrazinamide, see Scheme 1) is obtained as a derivative of L^2.

The crystal structure of L^2 (see Figure 1) reveals that its molecular backbone is not coplanar, with the mean deviation from the least-squares plane of 0.161 Å. The two terminal

Scheme 1. Solvothermal Formation of L^2 and $HL^4 \cdot H_2O$ from L^1 and Zn^{II}

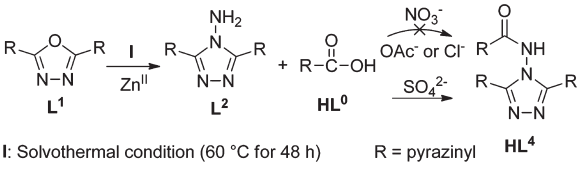

pyrazinyl groups deviate from the central triazole ring by the dihedral angles of 6.7 and 20.7°, respectively, and the dihedral angle between them is 27.3°. In addition, the angles subtended at the center of triazole ring (X) and two pyrazinyl *N*-donors are 109.0° for N1−X−N7 and 174.1° for N2−X−N8. Interestingly, the amino group affords a pair of intramolecular N−H···N bonds with the adjacent pyrazinyl groups (see Table S2, Supporting Information for details), which effectively fix the *cisoid*-I conformation (see Scheme 2) of the L^2 molecule.

The crystal structure of $HL^4 \cdot H_2O$ (see Figure 2) indicates a *cisoid* conformation of the HL^4 molecule. The dihedral angles between the central triazole ring and the three pyrazinyl groups are 21.9, 5.7, and 61.8°, respectively. In addition, the HL^4 molecules are connected by the lattice aqua

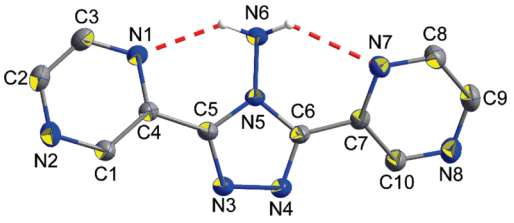

Figure 1. Molecular structure of $\mathbf{L^2}$ (ORTEP view at 30% thermal ellipsoids).

Scheme 2. Chemical Structures and Observed Conformations for $\mathbf{L^1}$, $\mathbf{L^2}$, $\mathbf{H_2L^3}$, and $\mathbf{HL^4}$

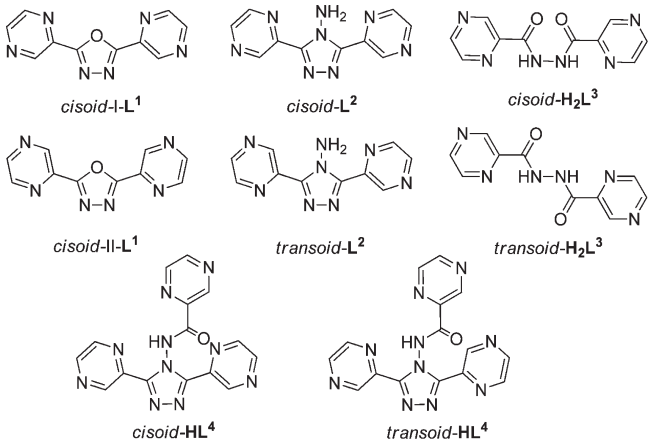

molecules to form a one-dimensional (1-D) H-bonding tape (see Figure S1, Supporting Information) along [100] via N6−H6A···O2, O2−H2B···O1, and O2−H2A···N3 interactions (see Table S2, Supporting Information for details).

In order to further validate the feasibility of such transformations from oxadiazole to triazole derivatives under solvothermal condition **I**, we have also taken the comparable reactions by using $\mathbf{L^1}$, H_3TMA, and different Zn^{II} salts. In such synthetic cases, two types of crystalline products $[(H_3TMA)\cdot(\mathbf{L^2})]$ (**1**) and $[(H_3TMA)\cdot(\mathbf{HL^4})]\cdot H_2O$ (**2**) are obtained when $Zn(NO_3)_2$ and $ZnSO_4$ are used, respectively (see Scheme 3), although the metal salts are not included in the resulting products, likewise those observed in the above reactions for generating $\mathbf{L^2}$ and $\mathbf{HL^4\cdot H_2O}$. From these results, we can conclude that the presence of Zn^{II} ion is most critical to such solvothermal transformations, which interestingly, are also dependent on the inorganic counteranions.

Compound **1** is a co-crystal[18] and in the local structure (see Figure 3), the $\mathbf{L^2}$ molecule is almost parallel to H_3TMA with a dihedral angle of 1.0°. The $\mathbf{L^2}$ molecule also adopts the *cisoid*-I conformation sustained by two intramolecular N−H···N bonds (see Table S2, Supporting Information). The dihedral angle between the two pyrazinyl groups is 8.6°, which make the dihedral angles of 2.6 and 6.1° with the central triazole ring. Each H_3TMA molecule forms four H-bonds with $\mathbf{L^2}$, and vice versa (i.e., O1−H1···N4, O3−H3···N8, O5−H5···N2, and N6−H6A···O4, see Table S2, Supporting Information), leading to the generation of three-dimensional (3-D) **cds** networks[19] that are of 2-fold interpenetration[20] (see Figure S2, Supporting Information).

In the structure of co-crystal compound **2** (see Figure 4), the $\mathbf{HL^4}$ component also displays the *cisoid* conformation, in which the three pyrazinyl groups are inclined to the central triazole system with dihedral angles of 9.0, 31.3, and 81.1°,

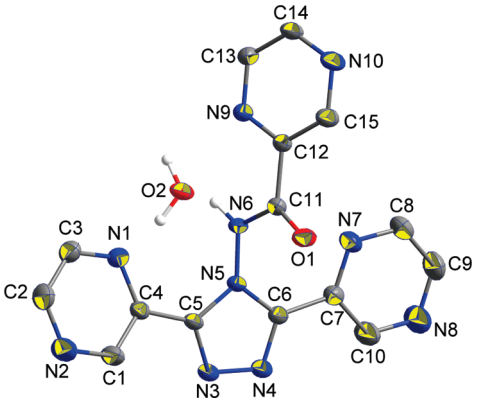

Figure 2. Molecular structure of $\mathbf{HL^4\cdot H_2O}$ (ORTEP view at 30% thermal ellipsoids).

Scheme 3. In Situ Solvothermal Syntheses of Compounds 1 and 2

$$H_3TMA + \mathbf{L^1} \xrightarrow[Zn(NO_3)_2]{\mathbf{I}} [(H_3TMA)\cdot(\mathbf{L^2})]\ (\mathbf{1})$$

$$H_3TMA + \mathbf{L^1} \xrightarrow[ZnSO_4]{\mathbf{I}} [(H_3TMA)\cdot(\mathbf{HL^4})]\cdot H_2O\ (\mathbf{2})$$

I: Solvothermal condition (60 °C for 48 h)

respectively. Notably, multiple hydrogen-bonding interactions exist involving the H_3TMA, $\mathbf{HL^4}$, and aqua components (see Table S2, Supporting Information). In detail, each H_3TMA is linked to three $\mathbf{HL^4}$, and vice versa (via N6−H6A···O3, O2−H2···N4, and O6−H6···N10), resulting in a 1-D ladder array (see Figure S3a, Supporting Information). Each aqua molecule serves as both H-bonding acceptor and donor to interact with two $\mathbf{HL^4}$ and one H_3TMA (O5−H5···O8, O8−H8A···N2, and O8−H8B···N8). Thus, the 1-D ladders are further extended into a 3-D supramolecular net (see Figure S3b, Supporting Information), in which H_2O, H_3TMA, and $\mathbf{HL^4}$ components can be considered as three-, four-, and five-connected nodes, respectively, to define a $(6^2.8)(4^2.6^2.8^2)(4^2.6^3.8^5)$ topology. Notably, two such 3-D nets are intertangled to result in a 2-fold interpenetrating framework (see Figure S3c, Supporting Information).

Compounds **1** and **2** were also characterized by ^1H NMR spectra in DMSO solution. The signals of phenyl/carboxyl protons of H_3TMA are similarly observed at 8.65/12.77 ppm for **1** and 8.62/12.82 ppm for **2**. Moreover, the presence of $-NH_2$ of $\mathbf{L^2}$ (for **1**) and −HN−C=O of $\mathbf{HL^4}$ (for **2**) can be confirmed by the NMR peaks at 7.56 and 13.57 ppm, respectively. In addition, the C−H signals of pyrazinyl appear at 8.87/9.34 ppm for **1** and in the range of 8.73−9.35 ppm for **2**. The water molecule in compound **2** can also be identified by the signal at 4.68 ppm in the NMR spectrum.

In order to further explore the influence of metal ion on such conversions (from $\mathbf{L^1}$ to $\mathbf{L^2}$ or $\mathbf{HL^4}$), $CuSO_4$ and $Co(NO_3)_2$ are also used to react with $\mathbf{L^1}$ under solvothermal condition **I** (see Scheme 4). For such two cases, the in situ generation of two coordination complexes $\{[Cu_3(\mathbf{L^4})_2(SO_4)_2(H_2O)_3](H_2O)_9\}_n$ (**3**) and $[Co^{III}_2(\mathbf{L^3})_3](H_2O)_{7.5}$ (**4**) is observed. Notably, complex **4** can be isolated by the same procedure, using $CoCl_2$, $Co(OAc)_2$, or $CoSO_4$ as the Co^{II} source.

Different from the catalysis and/or template roles of Zn^{II} salts that are not involved in the final products for the solvothermal transformation from $\mathbf{L^1}$ to $\mathbf{L^2}$, $\mathbf{HL^4\cdot H_2O}$, **1**,

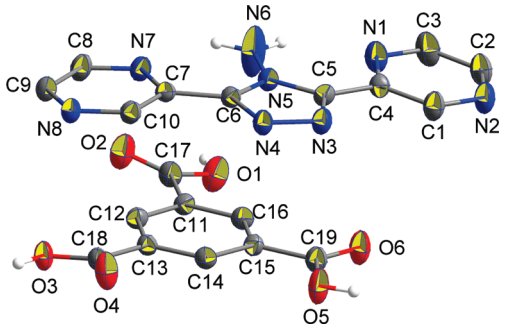

Figure 3. Molecular structure of **1** (ORTEP view at 30% thermal ellipsoids).

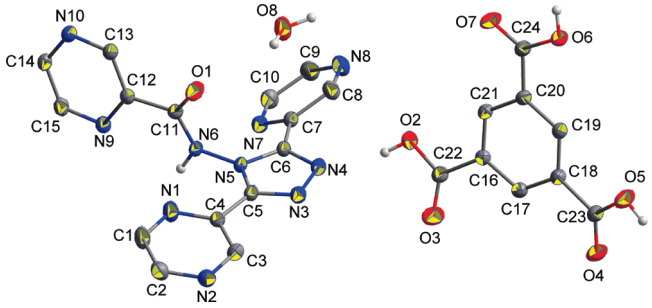

Figure 4. Molecular structure of **2** (ORTEP view at 30% thermal ellipsoids).

Scheme 4. Illustration of the Proposed Reaction Paths (Pink: Conventional Organic Syntheses,[13] Blue: the Cases of Zn^{II} Being not Involved in the Products, and Black: in Situ Metal/Ligand Reactions)

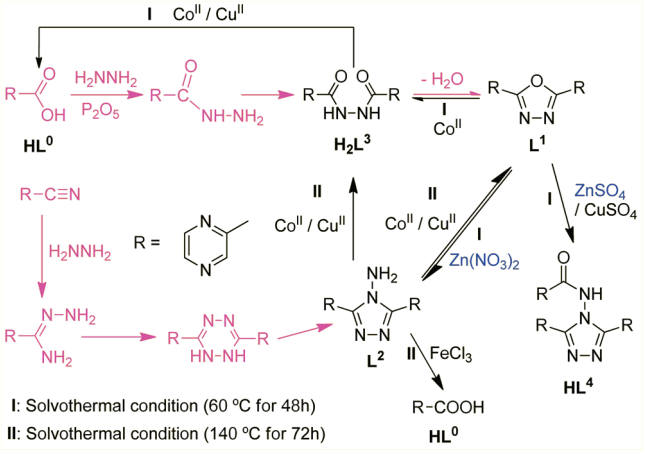

or **2**, $CuSO_4$ is found to coordinate with the in situ generated $\mathbf{L^4}$ ligand to form a 1-D coordination polymer **3**. In the asymmetric unit, three crystallographically independent Cu^{II} ions exist (see Figure 5a). Cu1 and Cu3 are similarly coordinated by four nitrogen donors from two $\mathbf{L^4}$ ligands as well as two oxygen atoms from one water and one sulfate to take a distorted octahedral sphere, and the Cu2 ion has a distorted square-pyramidal geometry ($\tau = 0.11$)[21] by coordinating to four nitrogen atoms from two $\mathbf{L^4}$ ligands and one axial water ligand. Notably, significant Jahn−Teller distortion is observed for both Cu1 and Cu3 (see Table S1, Supporting Information for detailed bond parameters). The two deprotonated anionic ligands $\mathbf{L^4}$ display the *transoid* conformation, each of which is connected to three Cu^{II} ions. As a result, a 1-D railway motif is formed along the [100] axis (see Figure 5b), in which the adjacent distances of Cu1···Cu2, Cu2···Cu3, and Cu1···Cu1/Cu3···Cu3 are 6.698, 6.614, and 7.529 Å, respectively.

Significantly, both metal oxidation and ligand hydrolysis are observed when $\mathbf{L^1}$ reacting with Co^{II} under the same condition, leading to the formation of a unique dimeric species **4**. In this structure, each octahedral Co^{III} ion is coordinated by three pairs of nitrogen atoms from three symmetry-related $\mathbf{L^3}$ ligands, and each *cisoid*-$\mathbf{L^3}$ displays a highly distorted configuration and bichelating coordination mode (see Figure 6). The dihedral angle between two pyrazinyl rings in $\mathbf{L^3}$ is 70.0° to properly meet the steric requirement for the formation of such a screwed motif, in which the Co^{III}···Co^{III} distance is 3.528 Å.

Transformation from the Triazole Derivative ($\mathbf{L^2}$). The above result clearly proves that the solvothermal generations of $\mathbf{L^2}/\mathbf{L^3}/\mathbf{L^4}$ are available from the $\mathbf{L^1}$ precursor with the assistance of metal ions. From the proposed reaction mechanism for conventional organic synthesis of $\mathbf{L^2}$ (see Scheme 4), the transformation from $\mathbf{L^2}$ to other derivates is also possible, although such reactions have not been observed.[12] To identify this viewpoint, we have carried out abundant trials, and fortunately the prospective results are achieved under the more vigorous reaction condition **II** (solvothermal, 140 °C for 72 h, see Scheme 4).

Reaction of $\mathbf{L^2}$, NH_4SCN, and $Co(NO_3)_2$ (or $CoSO_4$, $CoCl_2$, and $Co(OAc)_2$) under condition **II** affords a mononuclear coordination complex $[Co(\mathbf{L^1})_2(SCN)_2(H_2O)_2]\cdot(\mathbf{L^1})_2(H_2O)_6$ (**5**). Significantly, in this case, when NH_4SCN is excluded from the starting materials, only complex **4** can be isolated, which reveals its decisive role in such an in situ transformation process. The coordination unit of **5** has a discrete monomeric species with centrosymmetry (see Figure 7). Each Co^{II} ion, locating about an inversion center, is six-coordinated by four nitrogen atoms from two $\mathbf{L^1}$ and two SCN^- anions, and two aqua ligands to define an octahedral geometry. For both coordinated and lattice $\mathbf{L^1}$ molecules, the *cisoid*-I conformation is uniformly taken. Analysis of the crystal packing indicates a two-dimensional (2-D) layered pattern (see Figure S4, Supporting Information) constructed via multiple H-bonding contacts, involving the mononuclear unit, lattice water, and uncoordinated $\mathbf{L^1}$ (see Table S2, Supporting Information).

Treatments of $\mathbf{L^2}$ with Cu^{II} ($Cu(NO_3)_2$ for **6a** and $CuCl_2$ for **6b**) in the presence of NH_4SCN under solvothermal condition **II** afford two types of red block crystals $[Cu^{I}Cu^{II}(\mathbf{L^1})(\mathbf{L^3})(SCN)]_2(DMF)_2$ (**6a**) and $[Cu^{I}Cu^{II}(\mathbf{L^1})(\mathbf{L^3})(SCN)]_2(DMF)_2(H_2O)_2$ (**6b**). Notably, by using Cu^{II} acetate or sulfate also yields complex **6a**. For both **6a** and **6b**, the $\mathbf{L^2}$ ligands used in the above reactions are transformed to $\mathbf{L^1}$ and $\mathbf{L^3}$ at the same time, and the Cu^{II} ions are partly reduced to Cu^{I} centers, leading to the formation of novel mixed-valence tetranuclear complexes. The coexistence of both Cu^{II} and Cu^{I} ions can also be confirmed by the result of XPS (see Figure S5, Supporting Information).[22] In addition, complexes **6a** and **6b** represent a pair of pseudopolymorphs that only have a compositional difference of the lattice solvents.[23] In the structures of **6a** and **6b** (space groups $P\bar{1}$ and $C2/c$, respectively), two pairs of Cu^{II} and Cu^{I} ions are bridged by the $\mathbf{L^1}$ and $\mathbf{L^3}$ ligands to afford the tetranuclear core (see Figure 8), and the stereochemical arrangement of ligands and coordination geometry of

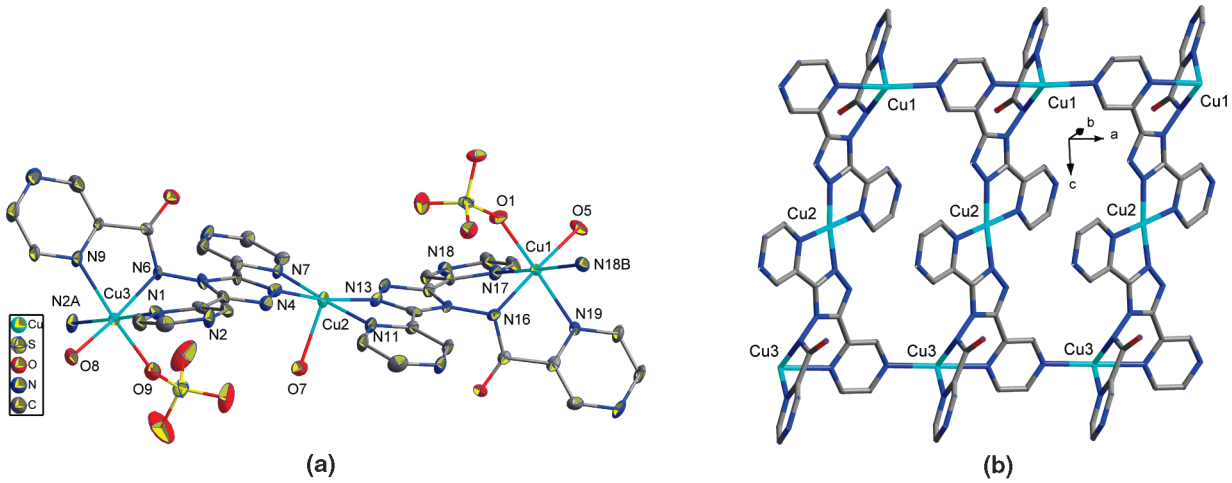

Figure 5. Views of **3**. (a) ORTEP view (30% thermal ellipsoids) showing the coordination environments of Cu^{II} (symmetry codes for A: $x-1$, y, z; B: $x+1$, y, z). (b) Portion view of the 1-D $[Cu_3(\mathbf{L}^4)_2]_n$ array (the water and sulfate ligands are omitted for clarity).

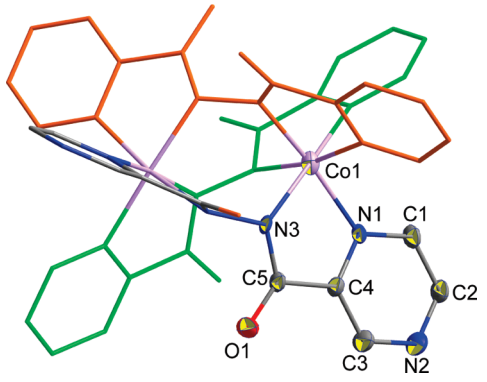

Figure 6. ORTEP view (30% thermal ellipsoids) of **4**, in which the uncoordinated water molecules are omitted for clarity.

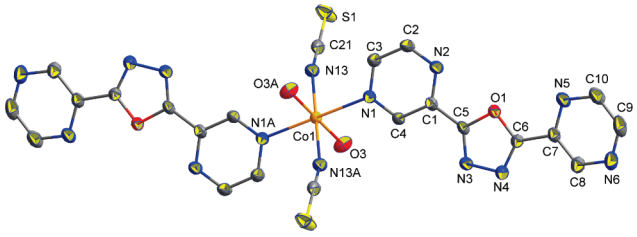

Figure 7. ORTEP view (30% thermal ellipsoids) of the coordination unit in **5** (symmetry code for A: $-x+1$, $-y+1$, $-z$).

metal centers are similar. In detail, the local coordination sphere (CuN_4O) of each Cu1 has a distorted square pyramidal configuration with the τ value of 0.22 for **6a** and 0.14 for **6b**. Each Cu2 is in a significantly distorted tetrahedral geometry and shows a typical structural character for univalent Cu ion.[24] Additionally, weaker Cu2−O2 and Cu2−N7 interactions are observed with their distances of 2.541/2.575 Å for **6a** and 2.836/2.312 Å for **6b**. As for the ligands, each *transoid* $\mathbf{L}^3$ in **6a** or **6b** shows a tridentate binding mode, and each $\mathbf{L}^1$ takes a bichelating fashion with *cisoid*-II conformation. In their tetranuclear motifs, the $Cu^I\cdots Cu^{II}$ distances separated by $\mathbf{L}^1/\mathbf{L}^3$ are 4.145/4.651 Å for **6a** and 4.070/4.692 Å for **6b**, respectively. It should be noted that a further analysis of the crystal packing of **6a** and **6b** indicates their completely different lattice arrangements. For **6a**, the tetranuclear units are well separated by DMF, whereas those in **6b** show an interlaced packing to form 1-D channels along [001], in which the lattice DMF and H_2O solvents are included (see Figure S6, Supporting Information). The potential voids for **6a** and **6b** (after eliminating the lattice solvents) are 292.4 and 2048.4 $Å^3$, corresponding to 20.5 and 31.4% of the respective unit-cell volume as evaluated by using the *PLATON* program.[25]

At this stage, compound $\mathbf{H_2L}^3$ may be proposed as the intermediate of the conversion reactions between $\mathbf{L}^1$ and $\mathbf{L}^2$. Especially, the Co^{III} complex **4** (with $\mathbf{L}^3$) can be obtained from both $\mathbf{L}^1$ and $\mathbf{L}^2$ via reacting with Co^{II} under different conditions. On the basis of these results, we have tried to isolate other coordination complexes of $\mathbf{L}^3$ from $\mathbf{L}^1$ or $\mathbf{L}^2$ and metal ions with variable valences (such as Fe, Mn, and Ni), using the similar in situ metal/ligand reactions. However, these trials are not successful, probably indicating the selectivity of Co^{II} for such a conversion. On the other hand, it has been known that the dipyridyl derivatives with oxadiazole spacer can suffer the solvothermal ring-open hydrolysis to in situ generate the corresponding pyridylcarboxylates in the presence of Zn^{II} or Cd^{II}.[26] In this context, by reacting $\mathbf{L}^2$ with $FeCl_3$ under condition **II**, a comparable in situ metal/ligand reaction occurs to afford a Fe^{II} complex $\{[Fe^{II}(\mathbf{L}^0)_2(H_2O)](H_2O)_2\}_n$ with pyrazinylcarboxylate ($\mathbf{L}^0$). This complex has been previously reported, which can be synthesized by assembly of Fe(III) perchlorate and $\mathbf{HL}^0$ in acetonitrile at room temperature with fully structural and magnetic characterizations.[27]

Role of Reaction Conditions. In our previous work, we have synthesized several Co^{II}, Cd^{II}, and Ag^I complexes with $\mathbf{L}^1$ under ambient conditions, and no comparable in situ metal/ligand reaction has been observed in the formation these coordination systems.[13a,28] Thus, it may be deduced that the solvothermal condition is necessary for the transformation of the oxadiazole ligand ($\mathbf{L}^1$) to other derivatives. In order to further demonstrate the effect of reaction condition on such in situ conversions of $\mathbf{L}^2$, we have attempted the reactions of Co^{II} or Mn^{II} with $\mathbf{L}^2$ and NH_4SCN under conventional conditions for a comparison. Here, the sources of Co^{II} and Mn^{II} (acetate, chloride, nitrate, or sulfate) are independent of the resulting products $[Co(\mathbf{L}^2)_2(SCN)_2]$ (**7**) and $[Mn(\mathbf{L}^2)(SCN)_2(H_2O)](H_2O)_2$ (**8**). The results also reveal the critical role of the reaction condition, especially for complexes **5** and **7** that can be obtained by using the same

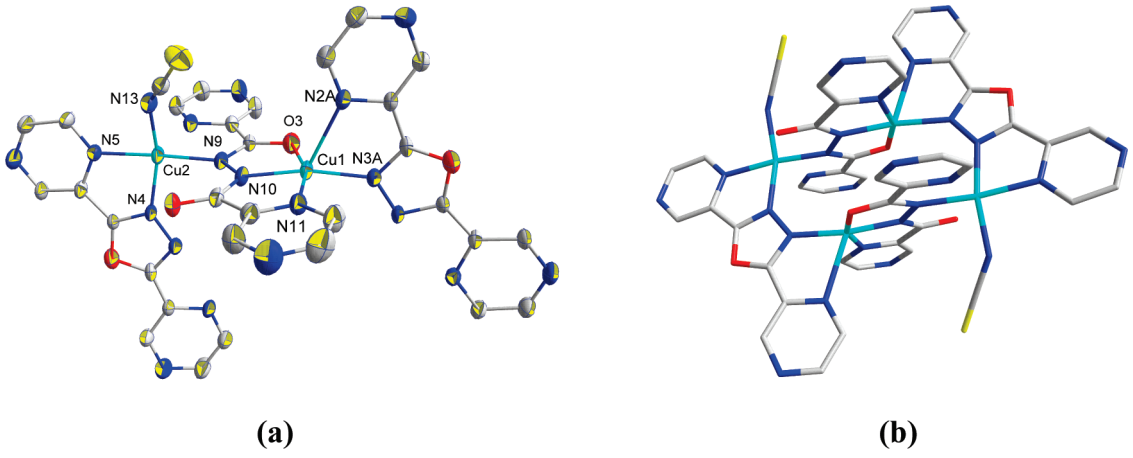

Figure 8. Views of **6b**. (a) ORTEP view (30% thermal ellipsoids) showing the coordination environments of Cu^{I} and Cu^{II} (symmetry code for A: $-x + 1/2, -y + 3/2, -z$). (b) Tetranuclear motif of $[Cu^{I}Cu^{II}(\mathbf{L}^{1})(\mathbf{L}^{3})(SCN)]_2$.

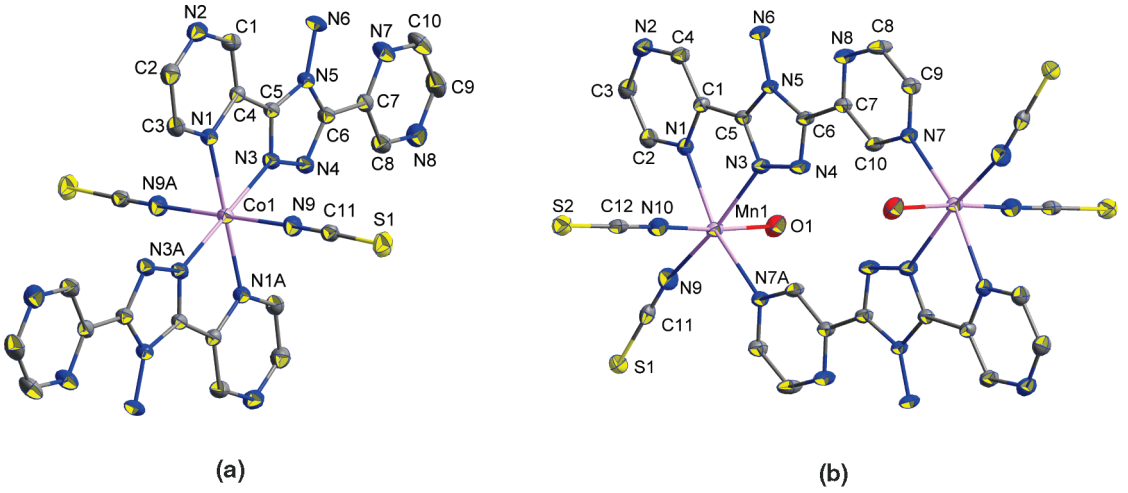

Figure 9. (a) ORTEP view (30% thermal ellipsoids) of **7** (symmetry code for A: $-x, -y + 1, -z$). (b) ORTEP view (30% thermal ellipsoids) of **8**, in which the uncoordinated aqua molecules are omitted for clarity (symmetry code for A: $-x + 2, -y + 1, -z + 2$).

starting reagent but under different solvothermal and conventional synthetic conditions.

In the structure of **7** (see Figure 9a), the octahedral sphere of Co^{II} is provided by six nitrogen donors from two cheating $\mathbf{L}^{2}$ ligands and two thiocyanate anions. Notably, $\mathbf{L}^{2}$ displays the *transoid* conformation with one pyrazinyl being uncoordinated, which is supported by intramolecular N6−H6A···N7 bond (see Table S2, Supporting Information). The resulting mononuclear motifs are further extended via intermolecular N6−H6B···N8 interactions to form 2-D corrugated layers (see Figure S7a, Supporting Information), which show a parallel stacking fashion (see Figure S7b, Supporting Information) in the 3-D crystalline lattice.

The Mn^{II} complex **8** shows a centrosymmetric dinuclear pattern (see Figure 9b), in which each Mn^{II} center is coordinated by five nitrogen donors of two $\mathbf{L}^{2}$ ligands and two thiocyanate anions, as well as one water molecule, adopting a distorted octahedral geometry. In this case, $\mathbf{L}^{2}$ also displays the *transoid* conformation supported by intramolecular N6−H6B···N8 bond, but with both pyrazinyl rings involved in metal coordination. Such a tridentate binding mode of $\mathbf{L}^{2}$ leads to the formation of a dimeric motif in which the Mn···Mn separation is 8.526 Å. Each dimeric coordination unit is linked to four adjacent motifs via N6−H6A···S2 and O1−H1A···S1 bonds to form a 2-D layer (see Figure S8a, Supporting Information). Additionally, the lattice water molecules serve as both H-bonding acceptors and donors (see Table S2, Supporting Information) to further extend such 2-D patterns into a 3-D supramolecular network (see Figure S8b, Supporting Information).

Magnetic Properties of the Co^{II} Complexes 5 and 7. The magnetic susceptibilities of **5** and **7** were measured in the temperature range of 2−300 K, and the results are shown in Figure S9 (Supporting Information) as χ_M and $\chi_M T$ vs T plots (χ_M is the molar magnetic susceptibility for one Co^{II} ion). The $\chi_M T$ values at 300 K are 2.35 $cm^3\ mol^{-1}\ K$ for **5** and 2.02 $cm^3\ mol^{-1}\ K$ for **7**, which are larger than the expected value for one isolated spin-only Co^{II} ion ($\chi_M T = 1.87\ cm^3\ mol^{-1}\ K$, $S = 3/2$). This is usually observed for Co^{II} complexes with the typical $\chi_M T$ values of 2.75−3.40 $cm^3\ mol^{-1}\ K$ arising from the contribution from orbital angular momentum at higher temperatures, and the lower values here indicate a perturbation from the ideal octahedral geometry of the Co^{II} ion.[29] Upon cooling, the $\chi_M T$ values continuously decrease to 1.21 $cm^3\ mol^{-1}\ K$ for **5** and 1.41 $cm^3\ mol^{-1}\ K$ for **7** at 2 K. The decrease of $\chi_M T$ with T should be ascribed to the intrinsic behavior of Co^{II}, instead of the antiferromagnetic interactions. In fact, as described above, both complexes are

mononuclear species and only hydrogen-bonding interactions exist between the coordinated entities with the long separations of the metal centers. This viewpoint can also be supported by the χ_M vs T plots for **5** and **7**, in which the χ_M values increase uniformly when the temperature is decreased, and no maximum is observed for both cases.

A Summary of the Conversion for the Dipyrazinyl Derivatives. At this stage, it is required to make a brief summary of the transformation for this series of dipyrazinyl species to further clarify the reaction mechanism thereof. As for the reaction of $\mathbf{L^1}$ (oxadiazole-based) under condition **I**, the Zn^{II} salts may be considered as the catalysts in the conversions from $\mathbf{L^1}$ to $\mathbf{L^2}$ or $\mathbf{HL^4}$ (triazole-based) and their binary co-crystals, which remarkably are anion dependent (SO_4^{2-} for $\mathbf{HL^4}$ species and others for $\mathbf{L^1}$ species). Such a conversion also rests with the metal ion, as indicated by the in situ generated Cu^{II} complex **3** (with $\mathbf{L^4}$) when $CuSO_4$ is used in a similar reaction. On the other hand, the inverse reaction pathway from $\mathbf{L^2}$ to $\mathbf{L^1}$ is also feasible under condition **II** (with a higher temperature/pressure and a longer time), as confirmed by complexes **5** and **6a**/**6b**. Significantly, both $\mathbf{L^1}$ and $\mathbf{L^3}$ ligands are observed in complexes **6a** and **6b**, representing a pair of pseudopolymorphs with very similar coordination structures but distinct packing fashions. Of further importance, complex **4** (with $\mathbf{L^3}$) can be in situ obtained from either $\mathbf{L^1}$ or $\mathbf{L^2}$ and Co^{II}. These results reveal that $\mathbf{L^3}$ should be the most possible intermediate of the interconversion between $\mathbf{L^1}$ and $\mathbf{L^2}$. Moreover, in situ metal/ligand reaction of Fe^{III} and $\mathbf{L^2}$ has also been found under condition **II** to afford a Fe^{II} complex with $\mathbf{L^0}$. Of course, all these conversions can only occur under solvothermal conditions, and the conventional reactions of $\mathbf{L^1}$ or $\mathbf{L^2}$ with different metal salts will only result in the corresponding complexes with the starting ligands, at least for all known examples so far.

The possible reaction mechanism for such conversions can be addressed as follows. Under condition **I**, from the hydrolysis of $\mathbf{L^1}$, the intermediate $\mathbf{H_2L^3}$ as well as $\mathbf{L^0}$ and hydrazine species can be directly obtained, which may further undergo nucleophilic addition to form $\mathbf{L^2}$ or $\mathbf{HL^4}$ and their related complexes in the presence of appropriate metal salts. Reversibly, the hydrazine component can also be eliminated from $\mathbf{L^2}$ under condition **II** to form $\mathbf{H_2L^3}$, from which $\mathbf{L^1}$ can be produced via cyclodehydration. Additionally, we have also explored the possible solvothermal transformations starting from $\mathbf{H_2L^3}$, aiming to obtain the in situ generated metal complexes with the related ligands. The results reveal that reactions of Cu^{II} or Co^{II} salts (nitrate and chloride) with $\mathbf{H_2L^3}$ under condition **I** afford two known mononuclear complexes $[M(\mathbf{L^0})_2(H_2O)_2]$ with $\mathbf{L^0}$,[30] and no identified solid product is found when the reactions are performed under condition **II**. This is unsurprising because $\mathbf{HL^0}$ is the precursor in synthesis of $\mathbf{H_2L^3}$, which can readily hydrolyze to result in $\mathbf{HL^0}$ and hydrazine. Even now, the in situ formation of other types of coordination systems cannot be precluded, due to the complexity of hydrothermal synthesis and crystallization, and such efforts under different reaction conditions are underway.

Conclusion

In summary, this work demonstrates that the dipyrazinyl derivatives with oxadiazole ($\mathbf{L^1}$) or triazole ($\mathbf{L^2}$) spacers can suffer interesting interconversions under appropriate solvothermal conditions with the assistance of metal ions. The possible existence of an intermediate $\mathbf{H_2L^3}$ has also been established, and significantly, these solvothermal reactions may be influenced by several factors such as reaction temperature, metal ion, and even inorganic counteranion used in syntheses. On the other hand, by accurately controlling the reaction conditions, a variety of coordination complexes (including mononuclear, dinuclear, tetranuclear, and polymeric species) and organic co-crystals with interesting supramolecular architectures can be obtained. Thus, these results will not only be useful to understand the mechanism and synthetic chemistry of organic azole systems but also reveal an effective strategy for the preparation of new crystalline materials.

Acknowledgment. This work was financially supported by the National Natural Science Foundation of China (Nos. 20671071, 20801042, and 20971098), Program for New Century Excellent Talents in University (No. NCET-07-0613), and Tianjin Normal University (No. 52X09004).

Supporting Information Available: Crystallographic data in CIF format, tables for bond parameters and H-bonding geometries, supplementary structural illustrations, XPS spectrum of **6b**, and temperature dependence of $\chi_M T$ and χ_M for **5** and **7**. This material is available free of charge via the Internet at http://pubs.acs.org.

References

(1) (a) Chen, X.-M.; Tong, M.-L. *Acc. Chem. Res.* **2007**, *40*, 162–170. (b) Cundy, C. S.; Cox, P. A. *Chem. Rev.* **2003**, *130*, 663–701. (c) Katritzky, A. R.; Nichols, D. A.; Siskin, M.; Murugan, R.; Balasubramanian, M. *Chem. Rev.* **2001**, *101*, 837–892. (d) Kitagawa, S.; Kitaura, R.; Noro, S. *Angew. Chem., Int. Ed.* **2004**, *43*, 2334–2375. (e) Abu-Shandi, K.; Winkler, H.; Wu, B.; Janiak, C. *CrystEngComm* **2003**, 180–189. (f) Ye, B.-H.; Tong, M.-L.; Chen, X.-M. *Coord. Chem. Rev.* **2005**, *249*, 545–565. (g) Feng, S.-H.; Xu, R.-R. *Acc. Chem. Res.* **2001**, *34*, 239–247. (h) Lu, J. Y. *Coord. Chem. Rev.* **2003**, *246*, 327–347.

(2) (a) He, J.; Yin, Y.-G.; Wu, T.; Li, D.; Huang, X.-C. *Chem. Commun.* **2006**, 2845–2847. (b) Cheng, J.-K.; Yao, Y.-G.; Zhang, J.; Li, Z.-J.; Cai, Z.-W.; Zhang, X.-Y.; Chen, Z.-N.; Chen, Y.-B.; Kang, Y.; Qin, Y.-Y.; Wen, Y.-H. *J. Am. Chem. Soc.* **2004**, *126*, 7796–7797. (c) Choi, J.; Gillan, E. G. *Inorg. Chem.* **2009**, *48*, 4470–4477. (d) Lu, J.; Bi, W.-H.; Xiao, F.-X.; Batten, S. R.; Cao, R. *Chem. Asian J.* **2008**, *3*, 542–547. (e) Su, C.-Y.; Goforth, A. M.; Smith, M. D.; Pellechia, P. J.; zur Loye, H. C. *J. Am. Chem. Soc.* **2004**, *126*, 3576–3586. (f) Chu, Q.; Liu, G.-X.; Huang, Y.-Q.; Wang, X.-F.; Sun, W.-Y. *Dalton Trans.* **2007**, 4302–4311. (g) Ye, Q.; Song, Y.-M.; Wang, G.-X.; Chen, K.; Fu, D.-W.; Chan, P.-W.; Zhu, J.-S.; Huang, S.-D.; Xiong, R.-G. *J. Am. Chem. Soc.* **2006**, *128*, 6554–6555. (h) Liu, C.-M.; Zuo, J.-L.; Zhang, D.-Q.; Zhu, D.-B. *CrystEngComm* **2008**, *10*, 1674–1680.

(3) (a) Duan, Z.; Zhang, Y.; Zhang, B.; Pratt, F. L. *Inorg. Chem.* **2009**, *48*, 2140–2146. (b) Amo-Ochoa, P.; Castillo, O.; Alexandre, S. S.; Welte, L.; de Pablo, P. J.; Rodriguez-Tapiador, M. I.; Gómez-Herrero, J.; Zamora, F. *Inorg. Chem.* **2009**, *48*, 7931–7936. (c) Kiebach, R.; Nather, C.; Sebastian, C. P.; Mosel, B. D.; Pottgen, R.; Bensch, W. *J. Solid State Chem.* **2006**, *179*, 3082–3086. (d) Ma, S.; Yuan, D.; Wang, X.-S.; Zhou, H.-C. *Inorg. Chem.* **2009**, *48*, 2072–2077. (e) Li, J.-R.; Tao, Y.; Yu, Q.; Bu, X.-H.; Sakamoto, H.; Kitagawa, S. *Chem.−Eur. J.* **2008**, *14*, 2771–2776. (f) Bauer, S.; Serre, C.; Devic, T.; Horcajada, P.; Marrot, J.; Férey, G.; Stock, N. *Inorg. Chem.* **2008**, *47*, 7568–7576. (g) Lan, A.-J.; Li, K.-H.; Wu, H.-H.; Kong, L.-Z.; Nijem, N.; Olson, D. H.; Emge, T. J.; Chabal, Y. J.; Langreth, D. C.; Hong, M.-C.; Li, J. *Inorg. Chem.* **2009**, *48*, 7165–7173. (h) Zhang, S.-S.; Zhan, S.-Z.; Li, M.; Peng, R.; Li, D. *Inorg. Chem.* **2007**, *46*, 4365–4367.

(4) (a) Ouellette, W.; Wang, G.-B.; Liu, H.-X.; Yee, G. T.; O'Connor, C. J.; Zubieta, J. *Inorg. Chem.* **2009**, *48*, 953–963. (b) Mahenthirarajah, T.; Li, Y.; Lightfoot, P. *Dalton Trans.* **2009**, 3280–3285.

(5) (a) Zhu, W.-H.; Wang, Z.-M.; Gao, S. *Inorg. Chem.* **2007**, *46*, 1337–1342. (b) Fang, Z.-L.; Yu, R.-M.; He, J.-G.; Zhang, Q.-S.; Zhao, Z.-G.; Lu, C.-Z. *Inorg. Chem.* **2009**, *48*, 7691–7697. (c) Wang, J.; Lin, Z.-J.; Ou, Y.-C.; Shen, Y.; Herchel, R.; Tong, M.-L. *Chem.−Eur. J.* **2008**, *14*, 7218–7235.

(6) (a) Zhao, X.-Q.; Zhao, B.; Shi, W.; Cheng, P.; Liao, D.-Z.; Yan, S.-P. *Dalton Trans*. **2009**, 2281–2283. (b) He, H.-Y.; Dai, F.-N.; Sun, D.-F. *Dalton Trans*. **2009**, 763–766. (c) Liu, Y.-Y.; Ma, J.-F.; Yang, J.; Ma, J.-C.; Su, Z.-M. *CrystEngComm* **2008**, *10*, 894–904. (d) Hu, S.; Tong, M.-L. *Dalton Trans*. **2005**, 1165–1167.

(7) (a) Zhang, X.-M. *Coord. Chem. Rev*. **2005**, *249*, 1201–1219. (b) Zhang, J.-P.; Zheng, S.-L.; Huang, X.-C.; Chen, X.-M. *Angew. Chem., Int. Ed*. **2004**, *43*, 206–209. (c) Tao, J.; Zhang, Y.; Tong, M.-L.; Chen, X.-M.; Yuen, T.; Lin, C.-L.; Huang, X.-Y.; Li, J. *Chem. Commun*. **2002**, 1342–1343. (d) Liu, C.-M.; Gao, S.; Kou, H.-Z. *Chem. Commun*. **2001**, 1670–1671. (e) Zhao, H.; Ou, Z.-R.; Ye, H.-Y.; Xiong, R.-G. *Chem. Soc. Rev*. **2008**, *37*, 84–100. (f) Lu, J. Y.; Cabrera, B. R.; Wang, R.-J.; Li, J. *Inorg. Chem*. **1998**, *37*, 4480–4481.

(8) (a) Schnurch, M.; Flasik, R.; Khan, A. F.; Spina, M.; Mihovilovic, M. D.; Stanetty, P. *Eur. J. Org. Chem*. **2006**, 3283–3307. (b) Crabtree, R. H. *J. Organomet. Chem*. **2005**, *690*, 5451–5457. (c) Haasnoot, J. G. *Coord. Chem. Rev*. **2000**, *200*, 131–185. (d) Klingele, M. H.; Brooker, S. *Coord. Chem. Rev*. **2003**, *241*, 119–132. (e) Beckmann, U.; Brooker, S. *Coord. Chem. Rev*. **2003**, *245*, 17–29.

(9) (a) Venkatakrishnan, K.; von Moltke, L. L.; Greenblatt, D. J. *Clin. Pharmacokinet*. **2000**, *38*, 111–180. (b) Singh, H.; Chawla, A. S.; Kapoor, V. K.; Paul, D.; Malhotra, R. K. *Prog. Med. Chem*. **1980**, *17*, 151–183. (c) Hayakawa, Y.; Kawai, R.; Hirata, A.; Sugimoto, J.; Kataoka, M.; Sakakura, A.; Hirose, M.; Noyori, R. *J. Am. Chem. Soc*. **2001**, *123*, 8165–8176. (d) Ostrovskii, V. A.; Pevzner, M. S.; Kofmna, T. P.; Shcherbinin, M. B.; Tselinskii, I. V. *Targets Heterocycl. Syst*. **1999**, *3*, 467–526. (e) Hiskey, M.; Chavez, D. E.; Naud, D. L.; Son, S. F.; Berghout, H. L.; Bome, C. A. *Proc. Int. Pyrotech. Semin*. **2000**, *27*, 3–14.

(10) (a) Du, M.; Bu, X.-H. *Bull. Chem. Soc. Jpn*. **2009**, *82*, 539−554 and references cited therein. (b) Du, M.; Zhang, Z.-H.; Zhao, X.-J.; Xu, Q. *Inorg. Chem*. **2006**, *45*, 5785–5792. (c) Bu, X.-H.; Liu, H.; Du, M.; Zhang, L.; Guo, Y.-M.; Shionoya, M.; Ribas, J. *Inorg. Chem*. **2002**, *41*, 1855–1861. (d) Chen, X.-D.; Wu, H.-F.; Du, M. *Chem. Commun*. **2008**, 1296–1298. (e) Incarvito, C.; Rheihgold, A. L.; Qin, C.-J.; Gavrilova, A. L.; Bosnich, B. *Inorg. Chem*. **2001**, *40*, 1386–1390. (f) Dong, Y.-B.; Wang, H.-Y.; Ma, J.-P.; Shen, D.-Z.; Huang, R.-Q. *Inorg. Chem*. **2005**, *44*, 4679–4692.

(11) (a) Zhang, J.-P.; Chen, X.-M. *Chem. Commun*. **2006**, 1689–1699. (b) Kitchen, J. A.; Noble, A.; Brandt, C. D.; Moubaraki, B.; Murray, K. S.; Brooker, S. *Inorg. Chem*. **2008**, *47*, 9450–9458. (c) Yi, L.; Ding, B.; Zhao, B.; Cheng, P.; Liao, D.-Z.; Yan, S.-P.; Jiang, Z.-H. *Inorg. Chem*. **2004**, *43*, 33–43. (d) van Albada, G. A.; de Graaff, R. A. G.; Haasnoot, J. G.; Reedijk, J. *Inorg. Chem*. **1984**, *23*, 1404–1408. (e) Liu, J.-C.; Guo, G.-C.; Huang, J.-S.; You, X.-Z. *Inorg. Chem*. **2003**, *42*, 235–243.

(12) (a) Du, M.; Jiang, X.-J.; Zhao, X.-J. *Chem. Commun*. **2005**, 5521–5523. (b) Du, M.; Jiang, X.-J.; Zhao, X.-J. *Inorg. Chem*. **2006**, *45*, 3998–4006. (c) Du, M.; Jiang, X.-J.; Zhao, X.-J. *Inorg. Chem*. **2007**, *46*, 3984–3995. (d) Du, M.; Zhang, Z.-H.; You, Y.-P.; Zhao, X.-J. *CrystEngComm* **2008**, *10*, 306–321.

(13) (a) Du, M.; Zhao, X.-J.; Guo, J.-H.; Batten, S. R. *Chem. Commun*. **2005**, 4836–4838. (b) Bentiss, M. F.; Lagrenée, M.; Traisnel, M.; Mernari, B.; Elattari, H. *J. Heterocycl. Chem*. **1999**, *36*, 149–152.

(14) (a) Zhang, J.-P.; Lin, Y.-Y.; Huang, X.-C.; Chen, X.-M. *Dalton Trans*. **2005**, 3681–3685. (b) Zhang, J.-P.; Lin, Y.-Y.; Huang, X.-C.; Chen, X.-M. *Cryst. Growth Des*. **2006**, *6*, 519–523. (c) Cheng, L.; Zhang, W.-X.; Ye, B.-H.; Lin, J.-B.; Chen, X.-M. *Inorg. Chem*. **2007**, *46*, 1135–1143.

(15) *SAINT Software Reference Manual*; Bruker AXS: Madison, WI, 1998.

(16) Sheldrick, G. M. *SHELXTL NT Version 5.1. Program for Solution and Refinement of Crystal Structures*; University of Göttingen: Germany, 1997.

(17) X-ray quality crystals for $\mathbf{L^2}$ can also be obtained by the following approach: to a warming DMF solution (10 mL) of $\mathbf{L^2}$ (24 mg, 0.1 mmol) was added a water solution (10 mL) of $Zn(OAc)_2 \cdot 2H_2O$ (44 mg, 0.2 mmol) with vigorous stirring and heating at 80 °C for ca. 30 min. The resulting solution was filtered and allowed to stand at room temperature. Dark-brown lamellar crystals of $\mathbf{L^2}$ were collected after ca. one week upon solvent evaporation.

(18) For interpretation of co-crystal, see (a) Aakeröy, C. B.; Salmon, D. J. *CrystEngComm* **2005**, *7*, 439–448. (b) Moulton, B.; Zaworotko, M. J. *Chem. Rev*. **2001**, *101*, 1629–1658.

(19) For interpretation of the three-letter network codes, see O'Keeffe, M.; Peskov, M. A.; Ramsden, S. J.; Yaghi, O. M. *Acc. Chem. Res*. **2008**, *41*, 1782–1789.

(20) For interpretation of interpenetrating networks, see (a) Batten, S. R. *CrystEngComm* **2001**, *3*, 67–73. (b) Blatov, V. A.; Carlucci, L.; Ciani, G.; Proserpio, D. M. *CrystEngComm* **2004**, *6*, 377–395.

(21) Addison, A. W.; Rao, T. N.; Reedijk, J.; van Rijn, J.; Verschoor, G. C. *J. Chem. Soc., Dalton Trans*. **1984**, 1349–1356.

(22) (a) Hussain, Z.; Salim, M. A.; Khan, M. A.; Khawaja, E. E. *J. Non-Cryst. Solids* **1989**, *110*, 44–52. (b) Moretti, G.; Fierro, G.; Lo Jacono, M.; Porta, P. *Surf. Interface Anal*. **1989**, *14*, 325–336. (c) Jolley, J. G.; Geesey, G. G.; Haukins, M. R.; Wright, R. B.; Wichlacz, P. L. *Appl. Surf. Sci*. **1989**, *37*, 469–480. (d) Strohmeier, B. R.; Leyden, D. E.; Field, R. S.; Hercules, D. M. *J. Catal*. **1985**, *94*, 514–530.

(23) (a) Seddon, K. R. *Cryst. Growth Des*. **2004**, *4*, 1087–1087. (b) Desiraju, G. R. *Cryst. Growth Des*. **2004**, *4*, 1089–1090. (c) Nangia, A. *Cryst. Growth Des*. **2006**, *6*, 2–4.

(24) (a) Zhang, X.-M.; Tong, M.-L.; Gong, M.-L.; Lee, H. K.; Luo, L.; Li, K.-F.; Tong, Y.-X.; Chen, X.-M. *Chem.−Eur. J*. **2002**, *8*, 3187–3194. (b) Tong, M.-L.; Li, L.-J.; Mochizuki, K.; Chang, H.-C.; Chen, X.-M.; Li, Y.; Kitagawa, S. *Chem. Commun*. **2003**, 428–429. (c) Kuzelka, J.; Mukhopadhyay, S.; Spingler, B.; Lippard, S. J. *Inorg. Chem*. **2004**, *43*, 1751–1761.

(25) Spek, L. *J. Appl. Crystallogr*. **2003**, *36*, 7–13.

(26) (a) Du, M.; Guo, J.-H.; Zhao, X.-J. *J. Mol. Struct*. **2004**, *701*, 119–124. (b) Wang, Y.-T.; Fan, H.-H.; Wang, H.-Z.; Chen, X.-M. *Inorg. Chem*. **2005**, *44*, 4148–4150.

(27) Tanase, S.; Gallego, P. M.; Bouwman, E.; Long, G. J.; Rebbouh, L.; Grandjean, F.; de Gelder, R.; Mutikainen, I.; Turpeinen, U.; Reedijk, J. *Dalton Trans*. **2006**, 1675–1684.

(28) Du, M.; Li, C.-P.; Guo, J.-H. *Inorg. Chim. Acta* **2006**, *359*, 2575–2582.

(29) Telfer, S. G.; Sato, T.; Kuroda, R.; Lefebvre, J.; Leznoff, D. B. *Inorg. Chem*. **2004**, *43*, 421–429.

(30) (a) Klein, C. L.; Majeste, R. J.; Trefonas, L. M.; O'Connor, C. J. *Inorg. Chem*. **1982**, *21*, 1891–1897. (b) O'Connor, C. J.; Sinn, E. *Inorg. Chem*. **1981**, *20*, 545–551.